

The seepage transport of heavy metal Pb^{2+} through sand column in the presence of silicon powders

Bing Bai*, Zhenqian Zhai, Dengyu Rao

School of Civil Engineering, Beijing Jiaotong University, Beijing, 100044, P R China.

* Corresponding author. Tel.: +86 010 51684815. E-mail: bbai@bjtu.edu.cn

Abstract: The coupled transport of heavy metals with suspended particles has been a topic of growing interest. The main purpose of this study is to experimentally investigate the seepage transport of heavy metal Pb^{2+} in the presence of silicon powders (SPs) through a sand column under different seepage velocities ($v = 0.087\text{--}0.260$ cm/s), injection Pb^{2+} concentrations ($C_p = 0\text{--}800$ $\mu\text{g/ml}$) and SP sizes ($D_{50} = 2.8\text{--}25.5$ μm), which were likely to be encountered in practical engineering. The sand column was installed in a cylindrical chamber of 300 mm in length and 80 mm in internal diameter. The results clearly show that the increase in acidity results in a reduction of the repulsive interactions between SPs and the matrix, and consequently a decrease in the peak values in breakthrough curves (BTCs), especially for larger-sized SPs. The peak values and recovery rate of Pb^{2+} are obviously increased and an earlier breakthrough can be observed, due to the higher capacity of SPs with negative charge to adsorb heavy metal pollutants such as Pb^{2+} with positive charge. The adsorption of Pb^{2+} on SPs can reduce the repulsive forces between SPs and the matrix, thus resulting in the increase of the deposition possibility of SPs and the decrease of peak value and recovery rate.

Keywords: Seepage transport; Silicon powder; Heavy metal; Coupled effect; Sand column.

INTRODUCTION

The coupled transport of contaminants such as heavy metals, organic matters and radioactive materials with solid particles has been a topic of growing interest in a wide variety of fields, such as the filtration of colloidal particles, microbial pathogen-induced groundwater pollution, and bioremediation of contaminated groundwater aquifers in porous media (Chrysikopoulos et al., 2017; Porubcan and Xu, 2011; Sen and Khilar, 2006). Silicon powders (SPs) play an important role in soil and aquifer contamination and those SPs transported easily in the water flow can act as carriers of contaminants (Haliema et al., 2016; Kim and Walker, 2009). Oxides, clay minerals and colloidal organic particles that exist ubiquitously in the subsurface environment may make that the otherwise low mobile contaminants can more rapidly be transported towards greater depths and into ground and surface waters bodies due to their large specific surface area and high sensitivity to the physical and chemical environment (Sen and Khilar, 2006).

Contaminants in porous medium can be roughly classified into three types, including contaminants adsorbed on immobile solid particles, contaminants dissolved in water, and contaminants adsorbed on the surface of solid particles that move with water flow (Chrysikopoulos et al., 2017; Sen and Khilar, 2006). However, SPs can also be a barrier to the migration of contaminants if their presence clogs the porous medium (Bennacer et al., 2017; Li and Zhou, 2010; Natarajan and Kumar, 2011). Puls and Powell (1992) showed that the transport rate of colloid-associated arsenate (As) was more than 21-times that of dissolved As. Kersting et al. (1999) found that the radionuclides in the aquifers at the Nevada test site, where hundreds of underground nuclear tests were conducted, were associated with the colloidal component of the groundwater, and mobile colloids had the potential to enhance the transport of non-soluble contaminants due to the adsorption effect. Karathanasis (1999) also showed that the presence of colloids obviously enhanced metal (Cu and Zn) transport by 5- to 50-fold over that without colloids, with Zn being consistently more mobile than Cu. Yin et

al. (2010) investigated colloid-facilitated Pb transport in shooting range soils, and showed that there was a significant correlation between colloids and Pb in the leachates, and both the decrease in ionic strength and the increase in flow rate contributed to the release of colloids and Pb.

Generally, colloids provide a carrier for the rapid transport of heavy metals like Pb (Grolimund et al., 1996). Pang et al. (2005) studied the transport of bacteria-facilitated cadmium (Cd) by column experiments in a gravel aquifer, and discovered that the adsorption of Cd onto bacteria was positively related to solution pH, bacterial concentration and negative surface charge, but inversely related to Cd concentration. Missana et al. (2008) investigated the effect of the presence of bentonite colloids on the seepage migration of europium (Eu) and plutonium (Pu) in a granite environment, and found that the seepage migration of these radionuclides was mostly colloid driven. Wang et al. (2015) showed that illite colloids (<0.1 μm in size) did not influence As transport in sand columns due to their relatively low affinity for As, and humic acid substantially increased As transport because of the competition of humic acid against As for adsorptive sites on humic acid and potential formation of non-adsorbing aqueous phase As-humic acid complexes. Thus, clay-mineral colloids may not have a large potential to increase As transport. Ma et al. (2016) investigated the co-transport of soil colloids (<1.2 μm in size) and As at different pH and ionic strength in sand columns, and the results showed that the strong repulsion between the porous media and the soil colloids promoted As transport by blocking the adsorption of As onto the porous media, and the colloids acted not only as a carrier in facilitating solute transport but also as a barrier in the course of solute adsorption. Zhou et al. (2016) studied the co-transport of a single layer of graphene oxide (GO) particles and Cu^{2+} in granular natural sand columns, and concluded that GO had fairly high mobility and could serve as an effective carrier of Cu^{2+} .

Some mathematical models have been proposed to characterize the colloid-facilitated transport of contaminants in the dissolved phase (Sen and Khilar, 2006), which generally com-

prise the mass balance equations for solid particles and contaminants and the reaction processes among the constituents. Bekhit et al. (2009) studied the combined effect of colloids and bacteria on the contaminant transport and proposed a conceptual model considering multiple reactions, which was suitable for the case of three mobile constituents and a fixed solid matrix. Katzourakis and Chrysikopoulos (2014) also developed a mathematical model for the simultaneous transport of viruses and colloids in homogeneous porous media with uniform flow. Certainly, the feasibility of these mathematical models relies heavily on a good understanding of the coupled transport of multiple mobile and immobile species in aqueous phase. Overall, there is limited knowledge about the coupled transport of multiple components in porous media due to their complex physicochemical coupling behaviors.

Despite the recognized importance of the coupled transport of contaminants with solid particles like colloids due to their abundance in groundwater and particular physical properties such as large specific surface area and high adsorption capacity (Bai et al., 2017; Bekhit et al., 2009), surprisingly little is known about the coupled transport of contaminants with relatively larger solid particles with a median diameter of $>1 \mu\text{m}$.

The main objective of this research is to investigate the coupled transport of Pb^{2+} and SPs under different seepage velocities, injection Pb^{2+} concentrations and SP sizes in a porous medium consisting of sand columns. The variation of transport parameters such as the longitudinal dispersivity and deposition coefficient of SPs and the recovery rate of Pb^{2+} and SPs with the injected concentration of Pb^{2+} are discussed based on experimental results, and the coupled transport processes are analyzed using analytical solutions accounting for the release effect of the hydrodynamic deposition.

EXPERIMENTAL APPROACHES

Column setup

The sand column was installed in a cylindrical toughened Plexiglas chamber of 300 mm in length and 80 mm in internal diameter filled with quartz sands. Nylon membranes were placed at both ends of the sand column to obtain uniform seepage water and particle flow. A water tank was used to supply deionized seepage water. A peristaltic pump (LongerPump BT600-2J, Baoding, China; control range: 120–1200 ml/min) was used to provide constant water flow rates (i.e., 0.087, 0.173, and 0.260 cm/s). Flow water was pumped downwards through the vertical sand column, and the flow velocity was measured by a flow meter installed at the column inlet. The SP suspension with a given concentration of Pb^{2+} was injected using a 60-ml syringe at the column inlet.

Characteristics of the materials

Quartz sands (median diameter: $d_g = 2.2 \text{ mm}$; size range: 0.5–3.5 mm) were used as the porous material, in which the particles of 0.5–1 mm, 1–2 mm and 2–3.5 mm accounted for about 2.3%, 36.1% and 61.6%, respectively. These particles were pretreated with 0.01 mol/l of NaOH solution and 0.01 mol/l of HNO_3 solution in sequence to remove impurities, rinsed several times with deionized water, and oven-dried for 48 h at $105 \text{ }^\circ\text{C}$ prior to the experiments. The saturated sand column was packed in 3-cm increments with quartz sands mixed with deionized water to avoid air entrapment, and then vibrated cautiously by hand to ensure uniform packing. The water level was maintained a few centimeters above the sand surface. The measured density of the solid matrix was $\rho_s = 2.65$

$\pm 0.05 \text{ g/cm}^3$, and the porosity, which was defined as the ratio of the pore volume to the total column volume, was controlled in $n = 41.7\%$ when preparing a sample layer by layer. Four types of artificial spherical SPs (mainly composed of SiO_2) with a median diameter of $D_{50} = 2.8, 10.9, 18.7$ and $25.5 \mu\text{m}$ (i.e., dimensionless ratios $D_{50}/d_g = 0.0013\text{--}0.0116$) and a density of $\rho_s = 2.20 \text{ g/cm}^3$ were selected as injected particles. These particles had an unimodal particle size distribution (PSD), and the particle-size distribution was in the range of 1–80 μm measured by laser diffraction (LA-950 Mode, Horiba, Japan).

Operating procedure and measurement

The SP suspension with different particle ($C_{\text{inj}} = 1, 2, 4$ and 8 mg/ml) and Pb^{2+} ($C_p = 0\text{--}800 \mu\text{g/ml}$) concentrations was injected at Darcy velocities, v , of 0.087, 0.173, and 0.260 cm/s. The Reynolds numbers varied between 1.12 and 3.34, confirming that the experiments were conducted under laminar flow conditions (Alem et al., 2013; Bennacer et al., 2017). In each experiment, $V_{\text{inj}} = 30 \text{ ml}$ of SP suspension was injected in a pulse-injection fashion over a period of $t_{\text{inj}} = 2 \text{ s}$. The turbidity level in the effluent was measured three times and the means were used to minimize errors. All experiments were performed at room temperature of $22\text{--}24^\circ\text{C}$.

The transport process of SP suspension is complex (Tusara et al., 2015; Walshe et al., 2010; Xue et al., 2016) due to the mixed injection of contaminants like Pb^{2+} with SPs and the environmental change of seepage water (e.g., the variation of pH and Pb^{2+} concentration). Heavy metal Pb^{2+} ions exist generally under acidic conditions (e.g., $\text{pH} = 5.5$), and thus there is a need to investigate the effect of acidity on the coupled transport of SPs and Pb^{2+} . Two SP suspensions with different pH values were considered in this study. One suspension was neutral ($\text{pH} = 7$) and the other suspension was adjusted to $\text{pH} = 5.5$ by adding 0.01 mol/l of nitric acid (HNO_3) solution. The pH value of seepage water in the tank was the same as that of the injected suspension ($\text{pH} = 7$ or 5.5).

Various concentrations of Pb^{2+} solutions were prepared with powdered $\text{Pb}(\text{NO}_3)_2$ and deionized water, and the pH was adjusted to $\text{pH} = 5.5$ with 0.01 mol/l of NaOH solution. To estimate the effect of ionic strength (Na^+) caused by sample preparation, the transport processes of three concentrations of Pb^{2+} ($C_p = 100, 300$ and $500 \mu\text{g/ml}$) were investigated. The pH of the seepage water was the same as that of the injected solutions ($\text{pH} = 5.5$). The results show that a trace amount of Na^+ ions in Pb^{2+} solution has almost a negligible effect on the transport of Pb^{2+} .

The turbidity in the effluent was measured using a turbidity meter (2100N, HACH Co., USA; measurement range: 0–4000 Nephelometric Turbidity Units (NTU)) and then converted to particle concentration. The results show that there is a consistent relationship between particle concentration C [ML^{-3}] and turbidity N [NTU] for $\text{pH} = 5.5$ to 7, and thus the Pb^{2+} concentration of less than $800 \mu\text{g/ml}$ is used in this study. The concentration of Pb^{2+} dissolved in the solution was measured using an atomic absorption spectrophotometer (TAS-990G, Puxi Co., China; wavelength range: 190–900 nm). The Pb^{2+} absorbed on the surface of SPs in the effluent was extracted by adding 0.1 mol/l of EDTA (ethylenediaminetetraacetic acid disodium) in a constant temperature incubator (HZQ-F160, Baidian Co., China) and then centrifuged (Sigma 3K15, Minsks Co., Germany). The extraction efficiency of this method can be higher than 90 % (Fangueiro et al., 2002; Nedwed and Clifford, 2000).

Transport theory and parameters

A solution accounting for the release effect of the hydrodynamic deposition for variable concentration injection is used to simulate the experimental breakthrough curves (BTCs), and the outlet of SPs (or soluble heavy metals) in a uniform one-dimensional flow is analyzed by the following convection-dispersion partial differential equation (CDE) and deposition equation, respectively (Katzourakis and Chrysikopoulos, 2014; Simunek and van Genuchten, 2008):

$$\frac{\partial C(z,t)}{\partial t} = D \frac{\partial^2 C(z,t)}{\partial z^2} - u \frac{\partial C(z,t)}{\partial z} - \frac{\rho_s}{n} \frac{\partial \sigma(z,t)}{\partial t} \quad (1)$$

$$\frac{\rho_s}{n} \frac{\partial \sigma(z,t)}{\partial t} = k_d \cdot C(z,t) - k_r \cdot \frac{\rho_s}{n} \sigma(z,t) \quad (2)$$

where z is the coordinate [L], n is the porosity of the porous medium, D is the hydrodynamic dispersion coefficient [$L^2 T^{-1}$], u is the average interstitial particle velocity [LT^{-1}], t is the time [T], σ is the concentration of particles deposited onto the solid matrix [MM^{-1}], k_d is the deposition coefficient [T^{-1}], and k_r is the release coefficient [T^{-1}].

The initial and boundary conditions are set as follows: $C(z,0) = 0$, $\sigma(z,0) = 0$, $C(0,t) = g(t)$, and $C(+\infty,t) = 0$. The particle concentration can be obtained from Eqs. (1) and (2) by the Laplace transform and the Laplace transform inversion (Bai et al., 2017):

$$C(z,t) = \exp\left(\frac{uz}{2D}\right) \cdot \int_0^t g(\tau) \cdot \left[k_r \cdot W(z,t-\tau) + \frac{\partial W(z,t-\tau)}{\partial t} \right] d\tau \quad (3)$$

where τ is a dummy integration variable.

$$W(z,t) = \exp(-k_r t) \int_0^t I_0[2(\alpha\eta(t-\eta))^{1/2}] \cdot \frac{z}{2\eta\sqrt{\pi D\eta}} \cdot \exp\left[-\frac{z^2}{4D\eta} - \frac{u^2\eta}{4D} + (k_r - k_d)\eta\right] d\eta \quad (4)$$

$$\begin{aligned} \frac{\partial W(z,t)}{\partial t} = & \exp(-k_r t) \int_0^t \left\{ \left(\frac{\alpha\eta}{t-\eta}\right)^{1/2} I_1[2(\alpha\eta(t-\eta))^{1/2}] - \right. \\ & \left. k_r I_0[2(\alpha\eta(t-\eta))^{1/2}] \right\} \\ & \cdot \frac{z}{2\eta\sqrt{\pi D\eta}} \cdot \exp\left[-\frac{z^2}{4D\eta} - \frac{u^2\eta}{4D} + (k_r - k_d)\eta\right] d\eta + \\ & \exp(-k_r t) \cdot \frac{z}{2t\sqrt{\pi Dt}} \cdot \exp\left[-\frac{z^2}{4Dt} - \frac{u^2t}{4D} + (k_r - k_d)t\right] \end{aligned} \quad (5)$$

where α is an arbitrary constant, and I_0 and I_1 are the modified Bessel function of the first-kind of order zero and one, respectively.

For an instantaneous plane source with a particle concentration of $g(t)$ [ML^{-3}], one has:

$$g(t) = I \cdot \delta(t-t') \quad (6)$$

where $I = m/Q = m/(vA)$ is the strength of the plane source [MTL^{-3}], with m , Q and A being the mass of injected particles [M], the flow rate [L^3T^{-1}], and the column cross-sectional area [L^2], respectively; $\delta(\cdot)$ is the Dirac delta function; and t' is the moment of particle injection [T].

Note that $\int_{\alpha}^{\beta} f(t)\delta(t-\xi)dt = f(\xi)$ ($\alpha \leq \xi \leq \beta$), the substitution of Eq. (6) into Eq. (3) yields:

$$C(z,t-t') = \frac{I}{2\sqrt{\pi D}} \cdot A_1(z,t-t') \cdot \left\{ \int_0^{t-t'} A_2(t-t') \cdot A_3(z,\eta) \cdot A_4(z,\eta) d\eta + A_3(z,t-t') \cdot A_4(z,t-t') \right\} \quad (7)$$

where $A_1(z,t) = \exp\left(\frac{uz}{2D} - k_r t\right)$, $A_2(t) =$

$$\left(\frac{\alpha\eta}{t-\eta}\right)^{1/2} \cdot I_1[2(\alpha\eta(t-\eta))^{1/2}], \quad A_3(z,t) = \frac{z}{t^{3/2}}, \quad \text{and} \quad A_4(z,t) =$$

$$\exp\left[-\frac{z^2}{4Dt} - \frac{u^2t}{4D} + (k_r - k_d)t\right].$$

Eq. (7) can be used to simulate the BTCs of SPs for pulse injection, where the injection duration is sufficiently short to be considered instantaneous (Bennacer et al., 2017). Eq. (7) can be degenerated to the classical solution based on the convection-dispersion model by letting $k_r = 0$ and $t' = 0$. The simulated BTCs are obtained from Eq. (7) using Mathematica 9 (Wolfram Research). Here, the concept of dimensionless pore volume (PV) is introduced to describe the time process, which refers to the ratio of the total volume of water flowing through the sand column to the pore volume of the sand column. The dispersivity is defined as $\alpha_d = D/u_0$, where u_0 is the average interstitial fluid velocity ($u_0 = v/n$) (Bai et al., 2017). The recovery rate is defined by integrating simulated BTCs area:

$$R_e = \int_0^{\infty} Q C_{out}(t) dt / m \quad (8)$$

where R_e is the recovery rate (%).

Four parameters (particle velocity u , dispersivity α_d , deposition coefficient k_d , and release coefficient k_r) can be fitted using Eq. (7). However, it would be very difficult to estimate more than three parameters simultaneously. In order to circumvent this problem, it is assumed that $k_r = 0.1k_d$ (Bekhit et al., 2009; Katzourakis and Chrysikopoulos, 2014) because the release coefficient k_r is small as compared to the deposition coefficient k_d , such that only three parameters need to be identified. Overall, k_r has a nearly linear effect on R_e in a large range of k_r/k_d ratios (e.g., $k_r/k_d = 0.01-0.2$). For example, when $C_{inj} = 4$ mg/ml, $u_0 = 0.2$ cm/s, $u/u_0 = 0.8$, $\alpha_d = 0.3$ cm and $k_d = 0.04$ s $^{-1}$, R_e is increased from 49.6 % to 55.0% and then to 62.5 % as the k_r/k_d increases from 0.01 to 0.1 and then to 0.2.

RESULTS AND DISCUSSION

The effect of acidity on the transport of SPs

The relationships between the relative concentration C_R and PV for different injected concentrations of SPs (C_{inj}) are given in Figs. 1 and 2, where $v = 0.087$ cm/s and $v = 0.260$ cm/s. C_R is defined as $C_R = (C_{out} \cdot V_p)/m = (C_{out} \cdot V_p)/(C_{inj} \cdot V_{inj})$, where C_{out} and V_p are the particle concentration at the outlet and the pore volume of the entire soil column, respectively (Ahfir et al., 2009; Bai et al., 2017).

Obviously, the decline of pH (pH = 7 \rightarrow 5.5) results in more pronounced sorption deposition due to the increase of positive charge H^+ with the addition of HNO_3 . Actually, the pH of the suspension can have a significant effect on the surface charge properties of SPs and the matrix according to the Derjaguin-Landau-Verwey-Overbeek (DLVO) theory (Bennacer et al.,

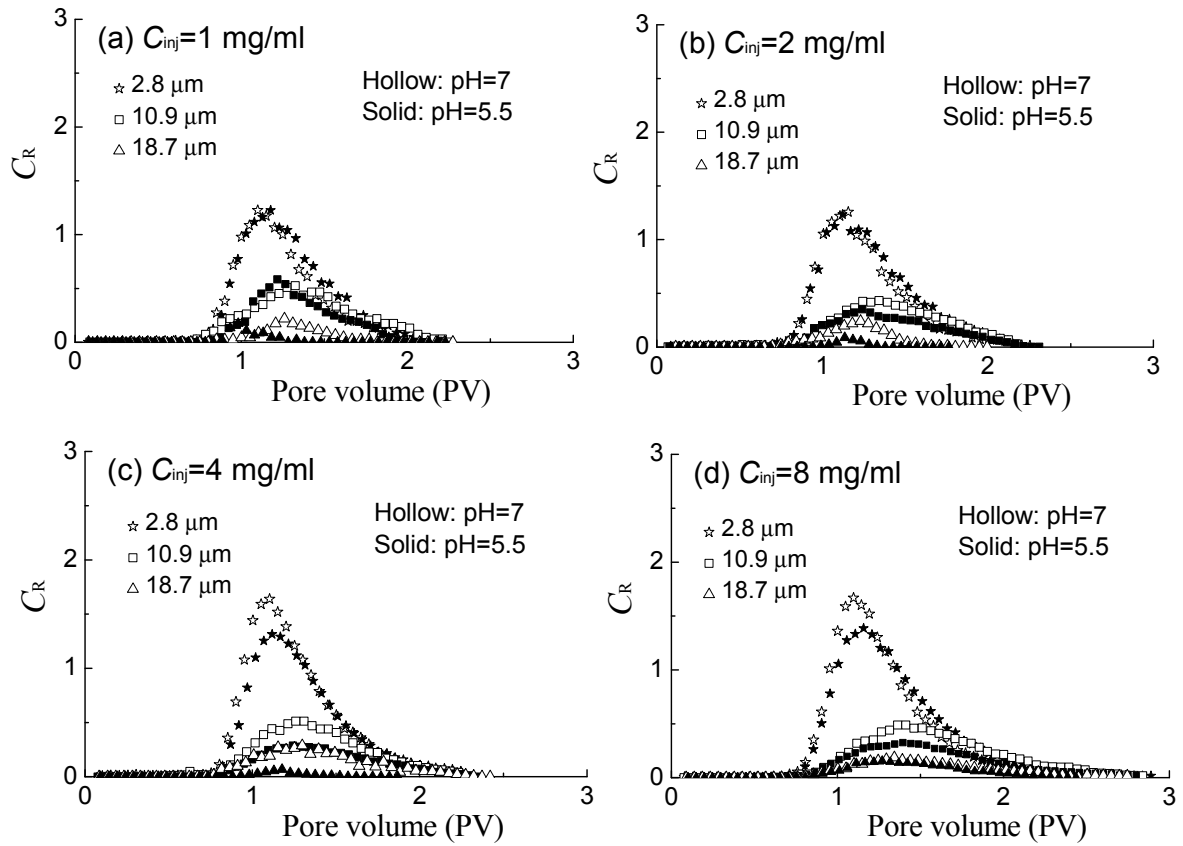


Fig. 1. BTCs of SPs at $v = 0.087$ cm/s for different SP sizes and acidity levels: (a) $C_{inj} = 1$ mg/ml, (b) $C_{inj} = 2$ mg/ml, (c) $C_{inj} = 4$ mg/ml, and (d) $C_{inj} = 8$ mg/ml.

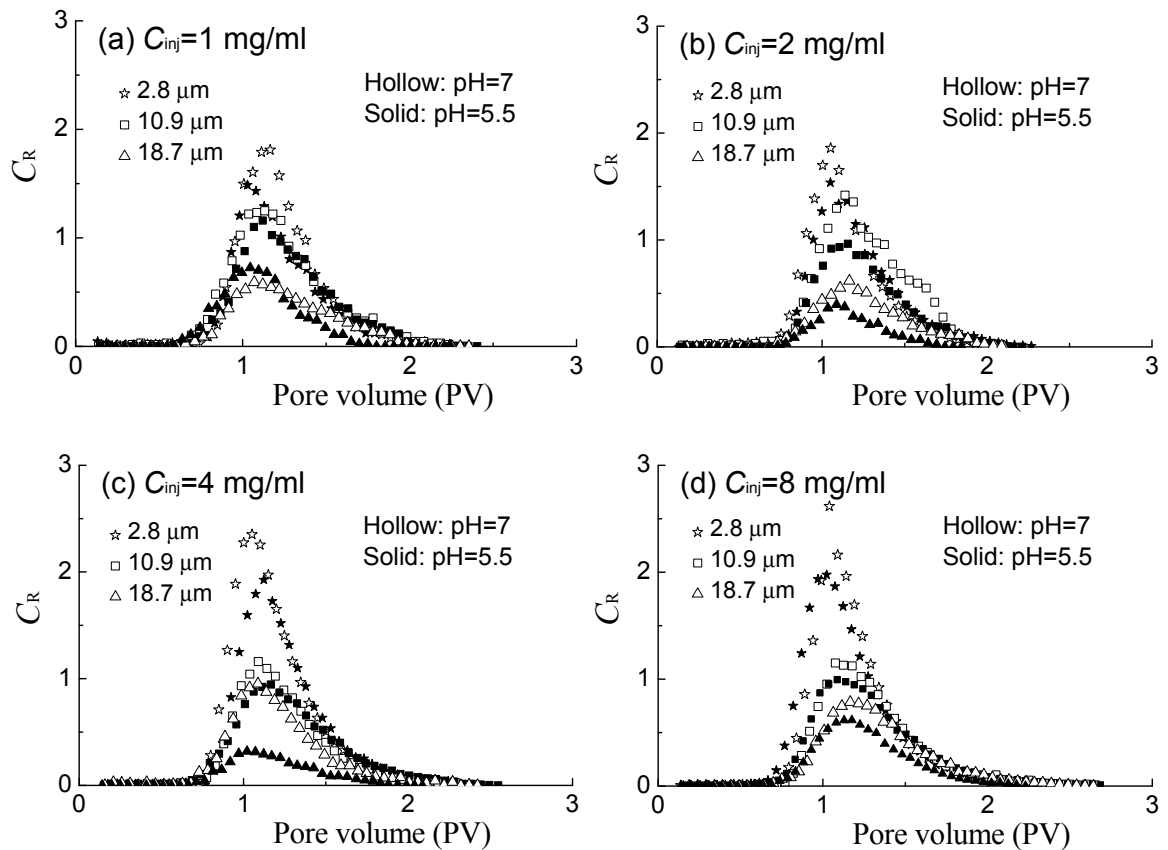


Fig. 2. BTCs of SPs at $v = 0.260$ cm/s for different SP sizes and acidity levels: (a) $C_{inj} = 1$ mg/ml, (b) $C_{inj} = 2$ mg/ml, (c) $C_{inj} = 4$ mg/ml, and (d) $C_{inj} = 8$ mg/ml

2017; Johnson et al., 2010; Tusara et al., 2015), and thus the deposition of SPs. Also, the increase of acidity (pH = 7→5.5) results in a reduction in the repulsive interactions between SPs and the matrix, and thus a decrease in peak value especially for SPs with a large size. For example, when $D_{50} = 2.8, 10.9$ and 18.7 (Fig. 1(c), $C_{inj} = 4$ mg/ml and $v = 0.087$ cm/s, the peak values are $C_R = 1.64, 0.51$ and 0.29 for pH = 7, and $C_R = 1.31, 0.29$ and 0.07 for pH = 5.5, respectively. Similar trends can be observed for different SP concentrations ($C_{inj} = 1, 2, 4$ and 8 mg/ml) and flow velocities ($v = 0.087, 0.173$ and 0.260 cm/s), which is also in good agreement with previous studies (e.g., Chrysikopoulos et al., 2017; Tusara et al., 2015). For example, Tusara et al. (2015) showed that decreasing the pH of the brine from 8 to 5.5 resulted in an increase in the deposition of suspended particles throughout the porous column and consequently a lower permeability along the porous column. Chrysikopoulos et al. (2017) found that the decrease of pH from 7 to 4 yielded smaller absolute zeta potentials and consequently smaller repulsion forces between SPs (e.g., graphene oxide nanoparticles and kaolinite particles) and the matrix (e.g., spherical glass beads and quartz sands).

The peak values decrease and the corresponding PVs increase slightly with increasing particles size ($D_{50} = 2.8 \rightarrow 10.9 \rightarrow 18.7$ μm ; see Figs. 1 and 2) at the same flow velocity. As discussed in detail elsewhere (e.g., Ahfir et al., 2009; Bradford et al., 2009), the number of the matrix pores larger than the particles decreases with increasing particle size, resulting in an increase in the number of particles captured by throat pores and a decrease of the peak values in the effluent.

The seepage transport of Pb^{2+}

Fig. 3 shows the penetration processes of Pb^{2+} ions under different concentrations and flow velocities. It shows that the

peak values of Pb^{2+} increase with increasing concentration of Pb^{2+} ($C_p = 100 \rightarrow 200 \rightarrow 300 \rightarrow 500$ $\mu\text{g/ml}$), but the corresponding PVs remain largely unchanged (PV = 1.04–1.08). It seems that unlike SPs, the peak occurrence of the BTCs of Pb^{2+} is independent of flow velocity. In fact, picometer-scale Pb^{2+} ions are completely soluble in water and move almost simultaneously with the water flow, which is mainly affected by the dispersivity and deposition effect. The so-called size exclusion effect makes the SP plume to have a lower effective dispersion coefficient than soluble Pb^{2+} due to the preferential advection of particles along the central streamline (Ahfir et al., 2009; Benacer et al., 2017). Moreover, the hydrodynamic force on the SPs increases with increasing water flow velocity, thus resulting in a decrease of deposition, and consequently an increase of the number of SPs at the outlet and the increase of peak values.

The transport processes of the heavy metal Pb^{2+} are also described using Eqs. (1) and (2). Fig. 4 gives the transport parameters of Pb^{2+} as a function of injection concentration obtained by fitting Eq. (7). All curves fit well with the experimental results ($R^2 > 0.92$) with only a few exceptions (e.g., see Fig. 3(a) and Fig. 3(b)). Fig. 4 shows that the moving velocity of Pb^{2+} ($u/u_0 = 0.71\text{--}0.84$; Fig. 4(a)) is always lower than the water flow velocity ($u/u_0 = 1$), and even lower than that ($u/u_0 = 0.85\text{--}0.90$) of two natural SiO_2 particles with $D_{50} = 25$ and 47 μm at a similar flow velocity of $v = 0.066\text{--}0.199$ cm/s in a previous study of Bai et al. (2017). Here, u/u_0 is defined as the ratio of the interstitial Pb^{2+} (or SPs) velocity u to the interstitial water velocity u_0 . In this sense, the moving velocity of Pb^{2+} is similar to that of a dissolved tracer (i.e., fluorescein) obtained by Bai et al. (2017), which is also in good agreement with many previous studies (Ahfir et al., 2009; Chrysikopoulos et al., 2017). This can be attributed to the tortuous transport paths of Pb^{2+} induced by its dispersivity and the obvious deposition of Pb^{2+} caused by high adsorption ability with the matrix. Fig. 4

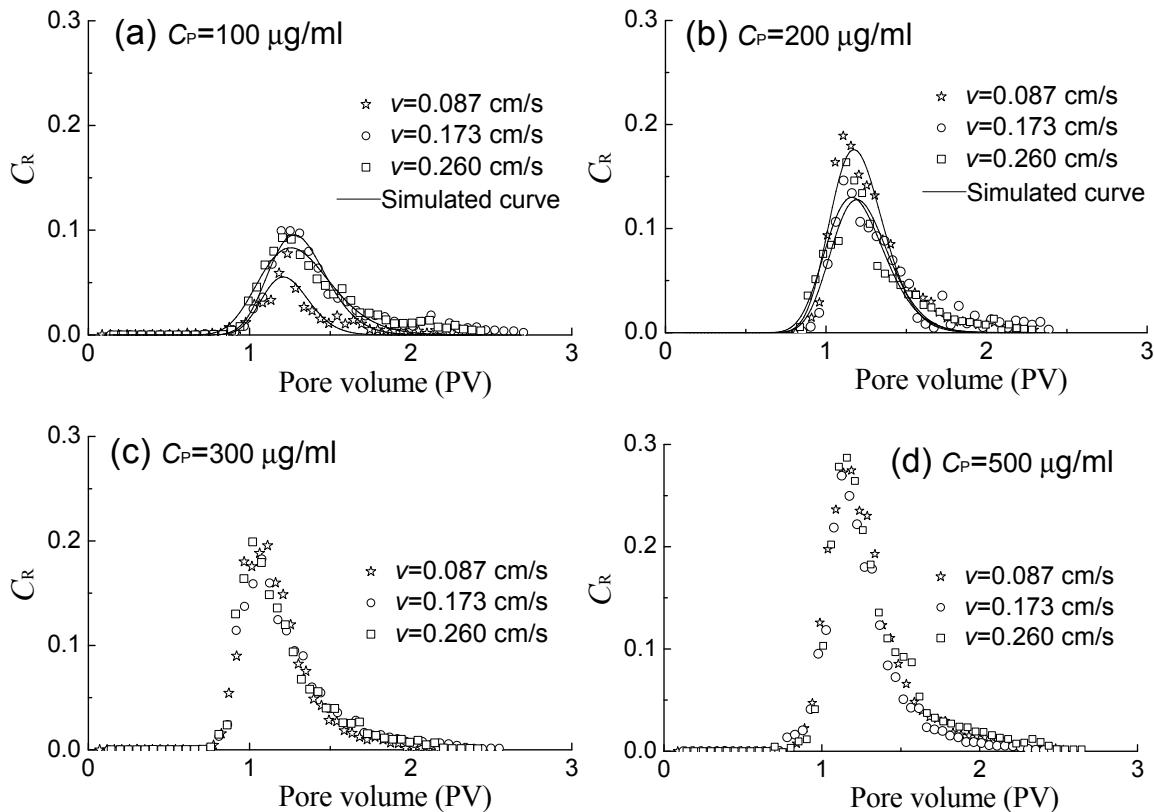


Fig. 3. BTCs of Pb^{2+} for various flow velocities: (a) $C_p = 100$ $\mu\text{g/ml}$, (b) $C_p = 200$ $\mu\text{g/ml}$, (c) $C_p = 300$ $\mu\text{g/ml}$, and (d) $C_p = 500$ $\mu\text{g/ml}$.

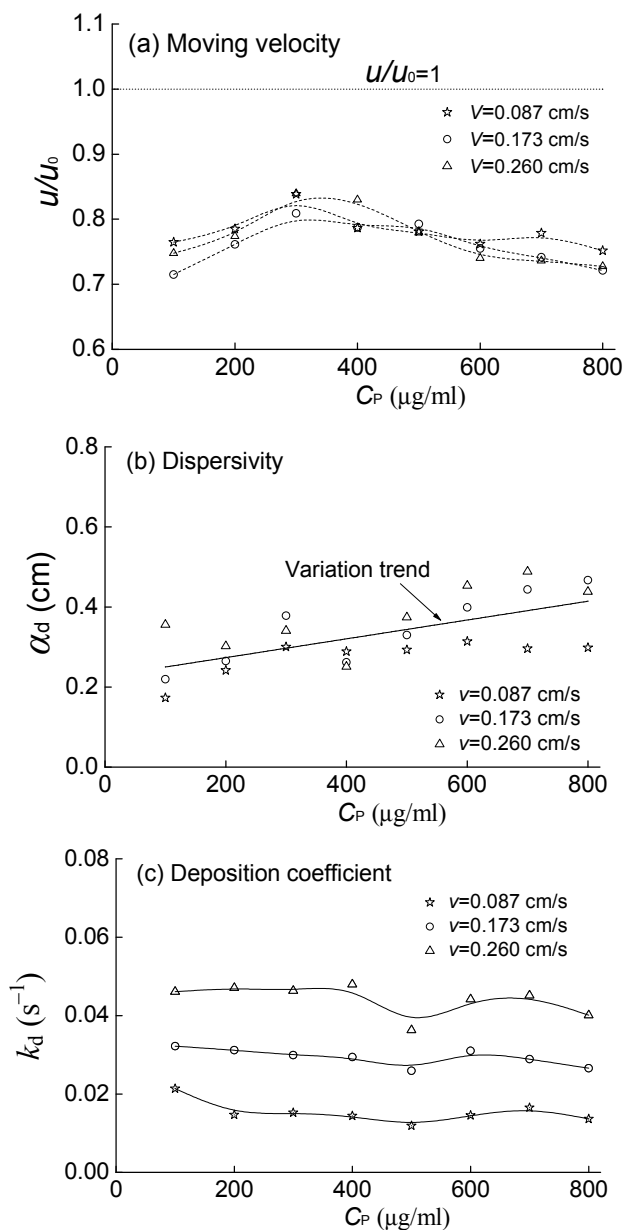


Fig. 4. The transport parameters of Pb^{2+} as a function of injection concentration: (a) moving velocity, (b) dispersivity, and (c) deposition coefficient.

also gives the experimental results and the variation of dispersivity α_d and deposition coefficient k_d with the Pb^{2+} concentration in the range of $C_p = 0$ – 800 $\mu\text{g/ml}$. It is evident that the dispersivity α_d is linearly related to the Pb^{2+} concentration (Fig. 4(b); $R^2 = 0.77$), regardless of the flow velocity due to its negligible effect. The dispersivity increases with the increase of C_p , resulting in a decrease in the moving velocity of Pb^{2+} to $u/u_0 = 0.72$ at a high concentration of e.g., $C_p = 800$ $\mu\text{g/ml}$ (Fig. 4(a)). However, the deposition coefficients decrease slightly with the increase of C_p (Fig. 4(c)), but increase with the increase of flow velocity. Actually, the existence of positive charge (i.e., H^+ and Pb^{2+}) in the solution makes the repulsive interactions between Pb^{2+} and the matrix to decrease with the decrease of the total interaction energy (i.e., the repulsive electrical double layer forces) by the DLVO theory (Porubcan and Xu, 2011). As a result, the decrease of the moving velocity of Pb^{2+} (u) and the increase of dispersivity (Fig. 4(b)) together induces apparent deposition (Fig. 4(c)), and the deposition coefficient is increased

by almost two times from $k_d = 0.014$ – 0.021 s^{-1} to $k_d = 0.036$ – 0.048 s^{-1} with the increase of the Darcy velocity from $v = 0.087$ cm/s to $v = 0.260$ cm/s.

The coupled transport of Pb^{2+} and SPs

The mixed suspension of Pb^{2+} and SPs are prepared following the same procedure as that of Pb^{2+} solution. Fig. 5 shows the transport of Pb^{2+} under three flow velocities ($v = 0.087$, 0.173 and 0.260 cm/s) and four SP sizes ($D_{50} = 2.8$, 10.9 , 18.7 and 25.5 μm) in the presence of SPs (called “coupled transport”, solid marks) or the absence of SPs (called “single transport”, hollow marks) at $\text{pH} = 5.5$, $C_p = 500$ $\mu\text{g/ml}$ and $C_{inj} = 2$ mg/ml, respectively. It can be seen from Fig. 5(a) that the peak values of Pb^{2+} are obviously increased due to the presence of SPs, and an earlier transport of Pb^{2+} with smaller PVs corresponding to peak values is observed, which can be attributed to the promotion effect of SPs on the transport of Pb^{2+} . It is well known that SPs with negative charge on their surfaces have a high capacity to adsorb heavy metal pollutants such as Pb^{2+} with positive charge. The SPs move with water flow (Li and Zhou, 2010; Natarajan and Kumar, 2011) and act as a third phase (mobile solid phase) in addition to the immobile solid phase of the porous media. Thus, Pb^{2+} can be adsorbed to SPs in a similar fashion as they do to the immobile solid matrix and can migrate in subsurface media at a rate similar to, or even greater than, that in the mobile aqueous phase due to the so-called size exclusion effect (Alem et al., 2013; Bai et al., 2017). Moreover, the penetration processes and the peak values also have nothing to do with flow velocity. Fig. 5 indicates that the peak values are $C_R = 0.40$, 0.51 , 0.44 and 0.36 in the presence of SPs for $D_{50} = 2.8$, 10.9 , 18.7 and 25.5 μm , respectively; but $C_R = 0.28$ on average in the absence of SPs. Here, the peak values are the mean values for the three velocities ($v = 0.087$, 0.173 and 0.260 cm/s).

The so-called promotion effect was previously observed in the coupled transport of colloids of < 1 μm in size with various contaminants such as alkali and alkaline earth cations (Cs^+ and Sr^{2+}), transition metals (Ni^{2+} , Co^{2+} , Cu^{2+} and Pb^{2+}), oxyanions (arsenic and iodate), and organic compounds (Bekhit et al., 2009; Chrysikopoulos et al., 2017; Katzourakis and Chrysikopoulos, 2014). The promotion or retardation of SPs on contaminants has been shown to depend on their coupled effect, the migration characteristics of SPs themselves, the hydrodynamic force, the physicochemical environment of suspension, etc. (Bekhit et al., 2009; Sen and Khilar, 2006). The existence of SPs with an appropriate size range (e.g., $D_{50} = 2.8$ – 10.9 μm ; Fig. 5(a) and Fig. 5(b)) can significantly accelerate the transport of Pb^{2+} due to the size exclusion effect. However, those SPs whose sizes exceed a limit (e.g., $D_{50} = 18.7$ μm , $D_{50}/d_g = 0.0085$; see the comparison of Fig. 5(b) and Fig. 5(c)) have only a small promotion effect or even an inhibition effect on the migration of Pb^{2+} due to the decrease of the permeability of porous medium caused by the plugging effect. For example, when $D_{50} = 25.5$ μm ($D_{50}/d_g = 0.0116$; Fig. 5(d)), the peak values of Pb^{2+} for $C_R = 0.36$ are only slightly higher than that for $C_R = 0.28$ in the absence of SPs, which is due to the remarkable deposition of large SPs onto the matrix (see Fig. 5(d)) despite the obvious absorption of Pb^{2+} on the SP surface. The plugging effect refers to the trapping of SPs in small pore throats that are too small to allow particle passage. Some researches indicated that this effect is mainly related to a threshold of D_{50}/d_g which is about in the range of $D_{50}/d_g = 0.0016$ – 0.027 (Alem et al., 2013; Bradford et al., 2009; Porubcan and Xu, 2011; Shen et al., 2008),

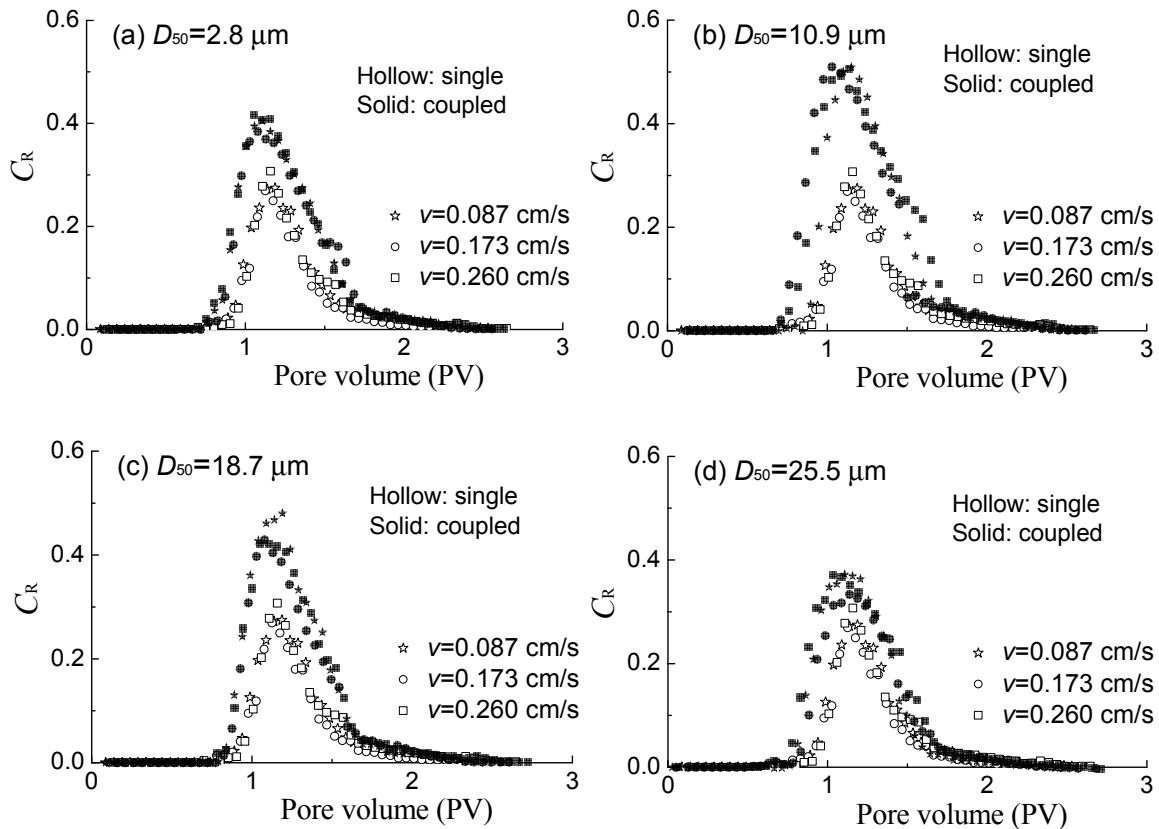


Fig. 5. BTCs of Pb^{2+} during the coupled transport with SPs: (a) $D_{50} = 2.8 \mu\text{m}$, (b) $D_{50} = 10.9 \mu\text{m}$, (c) $D_{50} = 18.7 \mu\text{m}$, and (d) $D_{50} = 25.5 \mu\text{m}$.

beyond which SPs will have a retardation effect on the transport of contaminants. The plugging effect is also related to the physical properties and particle-size distribution of SPs, the shape and surface roughness of the solid matrix, pore-scale hydrodynamics, the solution chemistry, etc.

Fig. 6 gives the BTCs for the coupled or single transport of SPs with different sizes at $\text{pH} = 5.5$, $C_p = 500 \mu\text{g/ml}$ and $C_{inj} = 2 \text{ mg/ml}$. Certainly, the peak values of SPs are decreased in the presence of Pb^{2+} , which seems to become more obvious at lower velocities (e.g., $v = 0.087 \text{ cm/s}$), especially for larger SP sizes (e.g., $D_{50} = 18.7 \mu\text{m}$; Fig. 6(c)). For example, when $D_{50} = 2.8 \mu\text{m}$ (Fig. 6(a)), the peak values are $C_R = 1.08, 0.89$ and 0.51 in the presence of Pb^{2+} and $C_R = 1.54, 1.42$ and 1.23 in the absence of Pb^{2+} for $v = 0.087, 0.173$ and 0.260 cm/s , respectively. The existence of Pb^{2+} absorbed on SPs can reduce the repulsive force between SPs and the matrix by the DLVO theory due to the change of surface charge properties of SPs and the matrix (i.e., the decrease of the absolute zeta potentials in theory) (Johnson et al., 2010; Tusara et al., 2015), and then enhance the deposition possibility of SPs onto the matrix. Hence, the coupled effect of Pb^{2+} with strong charge on SPs cannot be neglected, which is attributed to the decrease of the double electric layer on the SP surface (i.e., the decrease of surface potential energy).

There is an increasing interest in the effects of suspended particles like colloids and SPs on the seepage migration of contaminants like Pb^{2+} . However, the adsorption of contaminants on solid particles has attracted less attention, probably due to that the mass of contaminants adsorbed onto the solid particles can be negligible compared with the mass of solid particles. Actually, the participation of some specific contaminants will have an obvious effect on the transport of solid particles due to the change of their surface charge properties but cause no dramatic change in their mass. Unlike weak polar or

neutral contaminants, special attention should be given to the coupled effect on the transport of solid particles with heavy metal ions like Pb^{2+} with strong electric polarity. In essence, the influence of Pb^{2+} on the transport of solid particles is mainly determined by the change of the physicochemical environment of suspensions.

The effect of coupled process on transport parameters

Fig. 7 gives the values of particle velocity, dispersivity, deposition coefficient obtained by fitting Eq. (7) to observed BTCs (e.g., see Fig. 6(a) and Fig. 6(b)) and recovery rate of SPs using Eq. (8) under different flow velocities ($v = 0.087$ and 0.260 cm/s) and SP sizes ($D_{50} = 2.8, 10.9$ and $18.7 \mu\text{m}$) when the concentration of SPs is $C_{inj} = 2 \text{ mg/ml}$. $C_p = 0$ in Fig. 7 indicates the absence of Pb^{2+} . The coefficients of determination are $R^2 > 0.95$ except for few curves, and the variation trends in B-spline curves are also given. As mentioned before, the velocities of SPs ($u/u_0 = 0.80\text{--}1.00$) are generally higher than those of Pb^{2+} ($u/u_0 = 0.71\text{--}0.84$; see Fig. 4(a)), especially for those large-sized SPs (e.g., $D_{50} = 18.7 \mu\text{m}$) due to the size exclusion effect, indicating the earlier appearance of peak values (see Fig. 6). Moreover, the particle velocity slightly increases with the increase of Pb^{2+} concentration, which is partially caused by the enhancement of deposition due to the coupled action of Pb^{2+} (Fig. 6). The dispersivity of SPs decreases with the concentration of Pb^{2+} ($C_p = 0 \rightarrow 500 \mu\text{g/ml}$; Fig. 7(b)) and the SP size in the range of $D_{50} = 2.8\text{--}18.7 \mu\text{m}$, but increases with flow velocity ($v = 0.087 \text{ cm/s} \rightarrow 0.260 \text{ cm/s}$).

The deposition coefficient of SPs increases with increasing flow velocity ($v = 0.087 \rightarrow 0.260 \text{ cm/s}$) and SP size ($D_{50} = 2.8 \rightarrow 10.9 \rightarrow 18.7 \mu\text{m}$; Fig. 7(c)), which is in line with previous studies (Bai et al., 2017; Bennacer et al., 2017). More importantly, the deposition coefficient of SPs generally increases

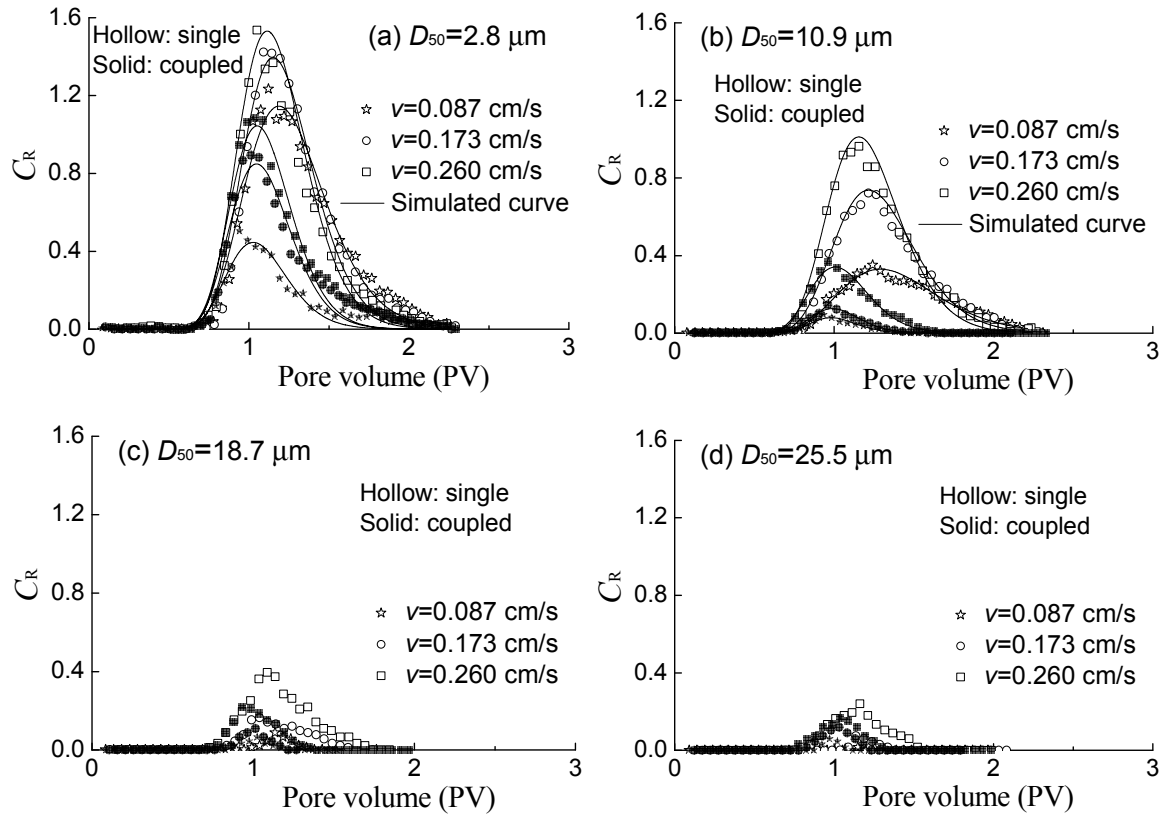


Fig. 6. BTCs of SPs during the coupled transport: (a) $D_{50} = 2.8 \mu\text{m}$, (b) $D_{50} = 10.9 \mu\text{m}$, (c) $D_{50} = 18.7 \mu\text{m}$, and (d) $D_{50} = 25.5 \mu\text{m}$.

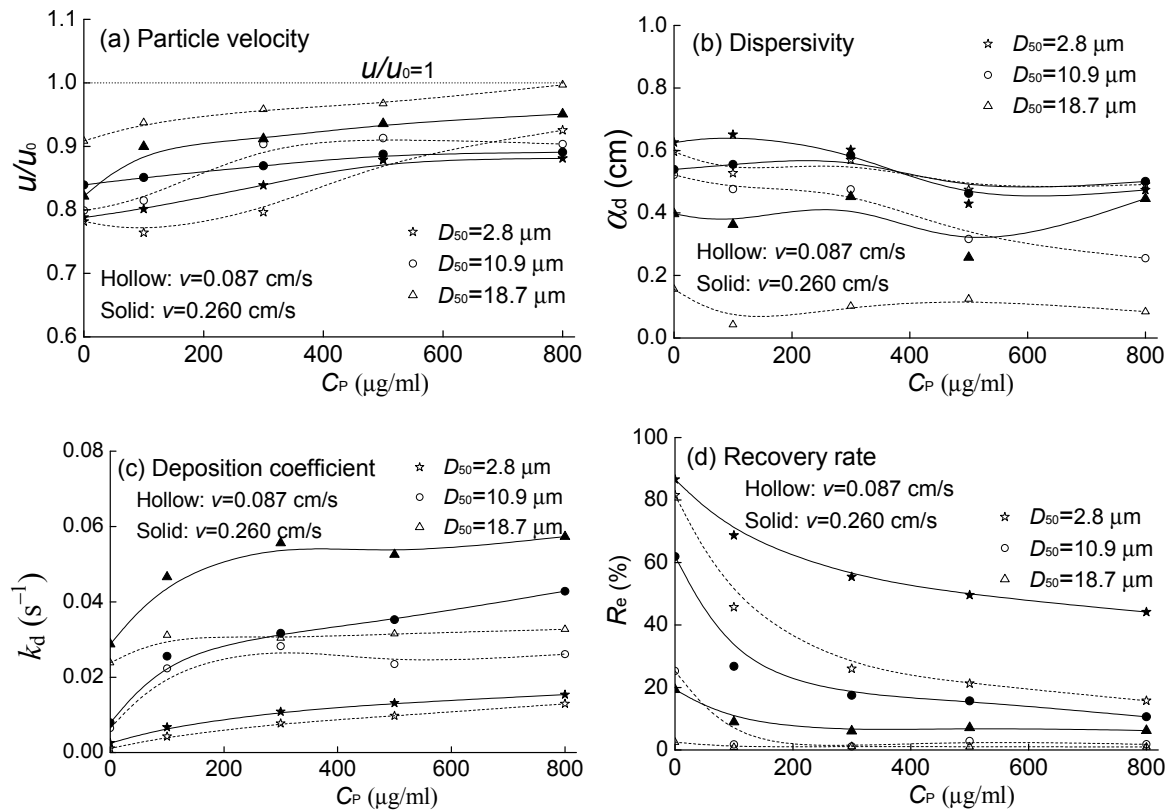


Fig. 7. The transport parameters of SPs during the coupled transport: (a) particle velocity, (b) dispersivity, (c) deposition coefficient, and (d) recovery rate.

with the injected concentration of Pb^{2+} and then remains almost constant, which is caused by the enhancement of the coupled effect (mutual adsorption) between SPs and Pb^{2+} and the obvious adsorption onto the surface of the matrix. As a result, the

recovery rate of SPs at the outlet decreases with the injected Pb^{2+} concentration and finally tends to be constant (Fig. 7(d)), indicating that caution must be taken when using single-transport parameters to predict the co-transport of SPs in the

presence of multiple components. Certainly, the recovery rate of SPs increases with the increase of flow velocity ($v = 0.087 \rightarrow 0.260$ cm/s; see Fig. 7(d)). When $v = 0.260$ cm/s, the recovery rates are to 44.1%, 10.6% and 6.2% for $C_p = 500$ $\mu\text{g/ml}$, and 86.6%, 61.9% and 19.3% for $C_p = 0$ when $D_{50} = 2.8$, 10.9, 18.7 μm , respectively.

By contrast, the recovery rate of Pb^{2+} is obviously increased from $R_e = 2.0$ –11.8% in the absence of SPs (hollow marks) to $R_e = 18.2$ –28.9% in the presence of SPs (solid marks; Fig. 8(a)) in the range of $C_p = 100$ –800 $\mu\text{g/ml}$ when $D_{50} = 2.8$ μm . However, the recovery rate of Pb^{2+} is independent of the flow velocity especially when $D_{50} = 2.8$ μm and 18.7 μm . Moreover, the recovery rate slightly increases with the injected concentration of Pb^{2+} and finally tends to be a steady value. However, it is noted that the steady state for SPs with a larger size can be achieved at a smaller C_p . For example, the steady values are approximately $C_p = 500$ and 300 $\mu\text{g/ml}$ for $D_{50} = 10.9$ and 18.7 μm , respectively (Fig. 8(b) and Fig. 8(c)).

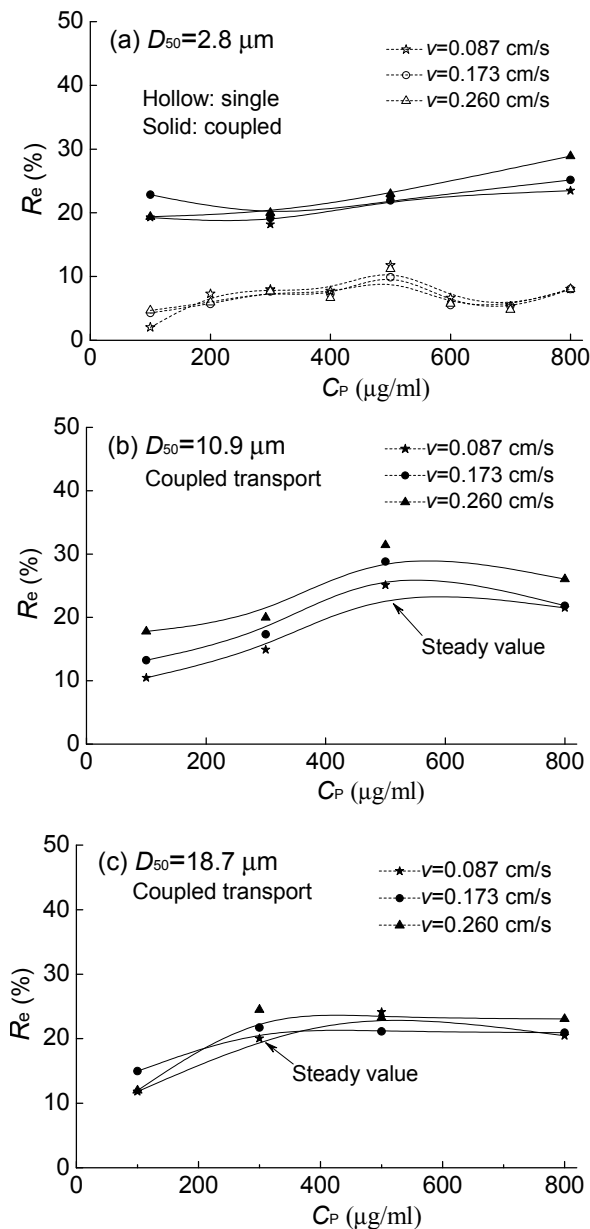


Fig. 8. Recovery rate of Pb^{2+} as a function of the injection concentration during the coupled transport with SPs: (a) $D_{50} = 2.8$ μm , (b) $D_{50} = 10.9$ μm , and (c) $D_{50} = 18.7$ μm .

CONCLUSIONS

The increase in acidity from $\text{pH} = 7$ to $\text{pH} = 5.5$ results in more pronounced sorption deposition due to the increase of positive charge H^+ with the addition of HNO_3 . Thus, the increase in acidity can reduce the repulsive interactions between SPs and the matrix, resulting in a decrease of the peak values in BTCs, especially for SPs with a large size.

For heavy metal ions such as Pb^{2+} , the peak values of BTCs increase with the increase of the injected Pb^{2+} concentration and are not related to flow velocity. With the increase of the injected concentration, the dispersivity increases and the deposition coefficient decreases slightly. The peak value and recovery rate of Pb^{2+} are obviously increased and an earlier breakthrough can be observed, due to the high capacity of SPs with negative charge to adsorb heavy metal pollutants such as Pb^{2+} with positive charge. The promotion or retardation of SPs on Pb^{2+} is closely related to the D_{50}/d_g value, which depends mainly on the coupled effect of Pb^{2+} and SPs, the transport characteristics of SPs themselves, the hydrodynamic force, the physicochemical environment of suspension, etc.

The adsorption of Pb^{2+} on SPs can reduce the repulsive forces between SPs and the matrix, thus resulting in the increase of the deposition possibility of SPs and the decrease of peak value and recovery rate.

Acknowledgements. This research was funded by the National Natural Science Foundation of China (51678043; 51878035) and National Key Basic Research Program of China (2015CB057800). The authors would like to thank Dr. Horst H. Gerke of Leibniz Centre for Agricultural Landscape Research for his constructive suggestions.

REFERENCES

- Ahfir, N.D., Benamar, A., Alem, A., Wang, H.Q., 2009. Influence of internal structure and medium length on transport and deposition of suspended particles: a laboratory study. *Transport in Porous Media*, 76, 2, 289–307.
- Alem, A., Elkawafi, A., Ahfir, N.D., Wang, H.Q., 2013. Filtration of kaolinite particles in a saturated porous medium: hydrodynamic effects. *Hydrogeology Journal*, 21, 573–586.
- Bai, B., Long, F., Rao, D.Y., Xu, T., 2017. The effect of temperature on the seepage transport of suspended particles in a porous medium. *Hydrological Processes*, 31, 2, 382–393.
- Bekhit, H.M., El-Kordy, M.A., Hassan, A.E., 2009. Contaminant transport in groundwater in the presence of colloids and bacteria: model development and verification. *Journal of Contaminant Hydrology*, 108, 152–167.
- Bennacer, L., Ahfir, N.D., Bouanani, A., Alem, A., Wang, H.Q., 2017. Coupled effects of ionic strength, particle size, and flow velocity on transport and deposition of suspended particles in saturated porous media. *Transport in Porous Media*, 118, 2, 251–269.
- Bradford, S.A., Kim, H.N., Haznedaroglu, B.Z., Torkzaban, S., Walker, S.L., 2009. Coupled factors influencing concentration-dependent colloid transport and retention in saturated porous media. *Environmental Science and Technology*, 43, 18, 6996–7002.
- Chrysikopoulos, C.V., Sotirelis, N.P., Kallithrakas-Kontos, N.G., 2017. Cotransport of graphene oxide nanoparticles and kaolinite colloids in porous media. *Transport in Porous Media*, 119: 181–204.
- Fangueiro, D., Bermond, A., Santos, E., Carapuca, H., Duarte, A., 2002. Heavy metal mobility assessment in sediments based on a kinetic approach of the EDTA extraction: search for optimal experimental conditions. *Analytica Chimica Acta*, 459, 2,

- 245–256.
- Grolimund, D., Borkovec, M., Barmettler, K., Sticher, H., 1996. Colloid-facilitated transport of strongly sorbing contaminants in natural porous media: a laboratory column study. *Environmental Science and Technology*, 30, 10, 3118–3123.
- Haliema, B., Zheng, H., Melson, N., Kaplan, D.L., Barnett, M.O., 2016. Decreased salinity and actinide mobility: colloid-facilitated transport or pH change. *Environmental Science and Technology*, 50, 625–632.
- Johnson, W.P., Pazmino, E., Ma, H., 2010. Direct observations of colloid retention in granular media in the presence of energy barriers, and implications for inferred mechanisms from indirect observations. *Water Research*, 44, 1158–1169.
- Karathanasis, A.D., 1999. Subsurface migration of copper and zinc mediated by soil colloids. *Soil Science Society of America Journal*, 63, 830–838.
- Katzourakis, V.E., Chrysikopoulos, C.V., 2014. Mathematical modeling of colloid and virus cotransport in porous media: application to experimental data. *Advances in Water Resources*, 68, 62–73.
- Kersting, A.B., Efurud, D.W., Finnegan, D.L., Rokop, D.J., Smith, D.K., Thompson, J.L., 1999. Migration of plutonium in ground water at the Nevada Test Site. *Nature*, 397, 56–59.
- Kim, H.N., Walker, S.L., 2009. *Escherichia coli* transport in porous media: influence of cell strain, solution chemistry, and temperature. *Colloids and Surfaces B: Biointerfaces*, 71, 1, 160–167.
- Li, Z.L., Zhou, L.X., 2010. Cadmium transport mediated by soil colloid and dissolved organic matter: a field study. *Journal of Environmental Sciences*, 22, 1, 106–115.
- Ma, J., Guo, H., Lei, M., Wan, X., Zhang, H., Feng, X., Wei, R., Tian, L., Han, X., 2016. Blocking effect of colloids on arsenate adsorption during co-transport through saturated sand columns. *Environmental Pollution*, 213, 638–647.
- Missana, T., Alonso, U., Garcia-Gutierrez, M., 2008. Role of bentonite colloids on europium and plutonium migration in a granite fracture. *Applied Geochemistry*, 23, 6, 1484–1497.
- Natarajan, N., Kumar, G.S., 2011. Spatial moment analysis of colloid facilitated radionuclide transport in a coupled fracture-matrix system. *International Journal of Energy and Environment*, 2, 3, 491–504.
- Nedwed, T., Clifford, D.A., 2000. Feasibility of extracting lead from lead battery recycling site soil using high-concentration chloride solutions. *Environmental Progress and Sustainable Energy*, 19, 3, 197–206.
- Pang, L., Close, M.E., Noonan, M., Flintoft, M., van den Brink, P., 2005. A laboratory study of bacteria-facilitated cadmium transport in alluvial gravel aquifer media. *Journal of Environmental Quality*, 34, 1, 237–247.
- Porubcan, A.A., Xu, S., 2011. Colloid straining within saturated heterogeneous porous media. *Water Research*, 45, 1796–1806.
- Puls, R.W., Powell, R.M., 1992. Transport of inorganic colloids through natural aquifer material: implications for contaminant transport. *Environmental Science and Technology*, 26, 3, 614–621.
- Sen, T.K., Khilar, K.C., 2006. Review on subsurface colloid and colloid-associated contaminant transport in saturated porous media. *Advances in Colloid and Interface Science*, 119, 2–3, 71–96.
- Shen, C., Huang, Y., Li, B., Jin, Y., 2008. Effects of solution chemistry on straining of colloids in porous media under unfavorable conditions. *Water Resources Research*, 44, 5, 335–342.
- Simunek, J., van Genuchten, M.T., 2008. Modeling nonequilibrium flow and transport processes using HYDRUS. *Vadose Zone Journal*, 7, 2, 782–797.
- Tusara, L., Itoi, R., Yamashiro, R., Fukuda, D., Kawahara, Y., 2015. Effects of suspended material and solution pH on solid deposition in porous media. *Journal of the Geothermal Research Society of Japan*, 37, 4, 143–152.
- Walshe, G.E., Pang, L.P., Flury, M., Close, M.E., Flintoft, M., 2010. Effects of pH, ionic strength, dissolved organic matter, and flow rate on the co-transport of MS2 bacteriophages with kaolinite in gravel aquifer media. *Water Research*, 44, 4, 1255–1269.
- Wang, Q., Cheng, T., Wu, Y., 2015. Distinct roles of illite colloid and humic acid in mediating Arsenate transport in water-saturated sand columns. *Water Air and Soil Pollution*, 226, 5, 1–15.
- Xue, S., Kong, X., Zhu, F., Hartley, W., Li, X., Li, Y., 2016. Proposal for management and alkalinity transformation of bauxite residue in China. *Environmental Science and Pollution Research*, 23, 13, 12822–12834.
- Yin, X., Gao, B., Lena, Q., Ma, L.Q., Saha, U.K., Sun, H., Wang, G., 2010. Colloid-facilitated Pb transport in two shooting-range soils in Florida. *Journal of Hazardous Materials*, 177, 620–625.
- Zhou, D.D., Jiang, X.H., Lu, Y., Fan, W., Hou, M.X., Crittenden, J.C., 2016. Cotransport of graphene oxide and Cu(II) through saturated porous media. *Science of the Total Environment*, 550, 717–726.

NOMENCLATURE

C	particle concentration
N	turbidity level
d_g	median diameter of porous materials
ρ_s	density of solid matrix or particles
n	porosity of porous materials
D_{50}	median diameter
C_{inj}	concentration of particle suspension
C_p	concentration of Pb^{2+} in particle suspension
v	Darcy velocity
V_{inj}	volume of suspended particle suspension in each injection
t_{inj}	sustained time of particle injection
z	coordinate
D	hydrodynamic dispersion coefficient
u	average interstitial particle velocity
t	time
σ	concentration of particles deposited onto the solid matrix
k_d	deposition coefficient
k_r	release coefficient
τ	dummy integration variable
α	arbitrary constant
I_0, I_1	modified Bessel function of the first kind of order zero and one
I	strength of the plane source
m	mass of particles injected
Q	water flow rate
A	cross-sectional area of column
$\delta(\cdot)$	Dirac delta function
ξ	dummy time
t'	particle injection moment
α_d	longitudinal dispersivity
u_0	average interstitial fluid velocity
PV	pore volume
R_e	recovery rate
C_R	relative concentration
C_{out}	particle concentration at the outlet
V_B	pore volume of the entire soil column
R^2	coefficient of determination

Received 14 March 2018
Accepted 9 October 2018